From Newton's bucket to rotating polygons

Journal:	*Journal of Fluid Mechanics*
Manuscript ID:	JFM-14-S-0216
mss type:	Standard
Date Submitted by the Author:	03-Mar-2014
Complete List of Authors:	Bach, Bjarne; Technical University of Denmark, Department of Physics & Center for Fluid Dynamics Linnartz, Erik; University of Twente, Physics of Fluids Group and J. M. Burgers Centre for Fluid Dynamics Vested, Malene; Technical University of Denmark, Department of Physics & Center for Fluid Dynamics Andersen, Anders; Technical University of Denmark, Department of Physics & Center for Fluid Dynamics Bohr, Tomas; Technical University of Denmark, Department of Physics & Center for Fluid Dynamics;
Keyword:	Waves/Free-surface Flows, Instability, Rotating flows < Geophysical and Geological Flows

Under consideration for publication in J. Fluid Mech.

From Newton's bucket to rotating polygons: experiments on surface instabilities in swirling flows

B. BACH[1], E. C. LINNARTZ[1,2], M. H. VESTED[1], A. ANDERSEN[1] AND T. BOHR[1]

[1]Department of Physics and Center for Fluid Dynamics, Technical University of Denmark, DK-2800 Kgs. Lyngby, Denmark

[2]Physics of Fluids Group and J. M. Burgers Centre for Fluid Dynamics, University of Twente, Enschede, The Netherlands

(Received 4 March 2014)

We present an experimental study of "polygons" forming on the free surface of a swirling water flow in a partially filled cylindrical container. In our set-up, we are able to rotate the bottom plate and the cylinder walls with separate motors, and thereby vary rotation rate and shear strength independently and move from a rigidly rotating "Newton's bucket" flow to one where bottom and cylinder walls are rotating oppositely and the surface is strongly turbulent but flat on average. Between those two extremes, we find polygonal states for which the rotational symmetry is spontaneously broken. We investigate the phase diagram spanned by the two rotational frequencies at a given water height and find polygons in a regime, where the two frequencies are sufficiently different and, predominantly, when they have opposite signs. In addition to the extension of the family of polygons found with the stationary cylinder, we find a new family of smaller polygons for larger rotation rates of the cylinder, opposite to that of the bottom plate. Further, we find a "monogon", a figure with one corner, roughly an eccentric circle rotating in the same sense as the cylinder. The case where only the bottom plate is rotating is compared to the results of Jansson *et al.* (Phys. Rev. Lett. **96**, 174502, 2006), where the same size of cylinder was used, and although the overall structure of the phase diagram spanned by water height and rotational frequency is the same, many details are different. To test the effect of small experimental defects, such as misalignment of the bottom plate, we study whether the rotating polygons are phase locked with the bottom plate, and although we find cases where the frequency ratio of figure and bottom plate is nearly rational, we do not find phase locking. On the other hand, we show that the system has a surprising multi-stability and excitability, and we suggest that this is the cause of the quantitative differences between the phase diagrams obtained in comparable experiments.

1. Introduction

Swirling flows with a free surface can undergo remarkable symmetry breaking transitions, where an originally rotationally symmetric surface spontaneously deforms into a rotating polygonal state (Vatistas 1990; Jansson *et al.* 2006; Suzuki *et al.* 2006) much akin to what is seen in the eyes of hurricanes (Lewis & Hawkins 1982) and on the north pole of Saturn (Godfrey 1988; Aguair *et al.* 2010). In the laboratory experiments, a cylindrical container is filled to a certain height with liquid (usually water) and the bottom

plate is rotated while the cylinder remains at rest (Vatistas 1990; Jansson *et al.* 2006; Suzuki *et al.* 2006; Tasaka & Iima 2009; Vatistas *et al.* 2008; Bergmann *et al.* 2011). Recently, Tophøj *et al.* (2013) have observed that the instability occurs quite generally when a fluid of low viscosity (e.g. liquid nitrogen undergoing film boiling) is set into rotation in a stationary container and slowly spins down, and it has been explained as a resonance between gravity waves and centrifugal waves. On the other hand, the famous Newton's bucket flow, where the entire cylinder and fluid volume is in rigid body rotation, and which was used by Newton to contrast inertial (non-rotating) reference frames with accelerated (rotating) ones, does not seem to give rise to any instabilities (Fabre & Mougel 2014).

In order to explore the symmetry breaking instability further, we have made an experimental set-up where we can independently control the rotation rates of the bottom plate and the cylinder and thereby vary rotation rate and shear rate independently. In this paper we present the first results from measurements with this set-up, in particular highlighting the region of the phase diagram, where instability can occur and the types of such instabilities. We shall first explain the set-up and then describe the phase diagram, firstly only rotating the bottom plate and secondly when we combine bottom plate and cylinder rotation. We shall compare our results when we only rotate the bottom plate with the older results of Jansson *et al.* (2006), and we show that although the overall features are the same, they differ in detail. To investigate possible reasons for these differences, we have measured the rotation rate of the polygons, in particular to rule out the possibility of phase locking between the bottom plate and the figure, which might have caused such differences. Finally, we show that there is a considerable multi-stability and excitability of the polygonal states, which might explain why small differences in set-up can cause changes in the phase diagram.

2. Experimental set-up

Our experimental set-up is shown in figure 1. A Plexiglas cylinder with inner diameter 29 cm has a Plexiglas bottom plate mounted 30 cm from the top rim such that both the cylinder and the plate can rotate independently, controlled by separate motors as shown in figure 1(a). The "bottom" plate is actually not placed at the bottom of the cylinder, but 10 cm above to let it rotate freely. The horizontal gap between the bottom plate and the cylinder is less than 1 mm and thus the fluid below the bottom plate does not play a role. Both the cylinder and the bottom plate can rotate with frequencies between 0.4 Hz and 6.9 Hz both clockwise and counter-clockwise. As shown in figure 1(b), the entire construction is large compared to the cylinder. The rack has dimensions of 120 cm $\times$ 80 cm $\times$ 250 cm, is made of aluminium, and weighs 140 kg. The vertical axis of rotation and the horizontal bottom plate are accurately set up, but the cylinder available to us has a slight skewness, introducing a wobbling of approximately 0.4°. To secure stability of the bottom plate and smoothness of its upper surface, we mounted it with screws from below to an attachment plate of the same size. We used two different bottom plates, one in black and one in white. The best pictures and visualisations are made with the white plate and a few drops of red dye to enhance the contrast. Figure 2 shows the three control parameters that we shall vary in the following, namely the rotational frequencies of the bottom plate, f_b, and of the cylinder, f_c, and the filling height of the water, H, i.e., the water height when both the bottom plate and the cylinder are at rest.

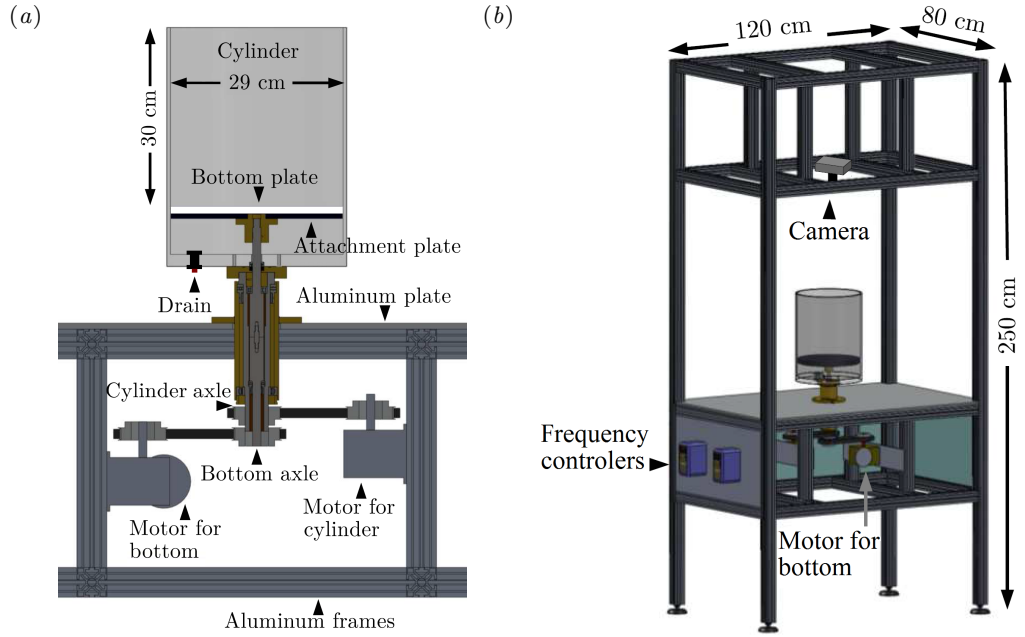

FIGURE 1. Sketches of the experimental set-up. (*a*) The Plexiglas cylinder and the bottom plate can rotate independently both in speed and direction. (*b*) The complete set-up with the embedding of the cylinder in a large and heavy aluminium construction which helps to stabilise the dynamics.

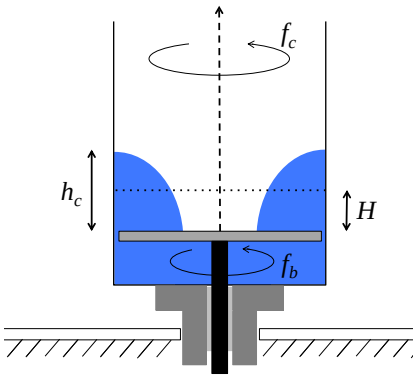

FIGURE 2. Sketch of the cylinder and bottom plate with parameters.

3. Polygons with rotating bottom and stationary cylinder

We first look at the case where the cylinder is stationary and only the bottom plate rotates. Typical polygonal states are shown in figure 3. This case has been studied earlier by Vatistas (1990) and Jansson *et al.* (2006) with whom we shall compare our results in section 5. To obtain a phase diagram, we vary the filling height of the water H from 30 mm to 80 mm with steps of 10 mm. For each water level the rotational frequency of the bottom plate f_b is increased from 0.4 Hz with steps of 0.1 Hz up to a value where no more polygons are seen and the states regain the rotational symmetry. Every time the frequency is increased, we wait 1 minute to let the flow equilibrate to what seems to be the

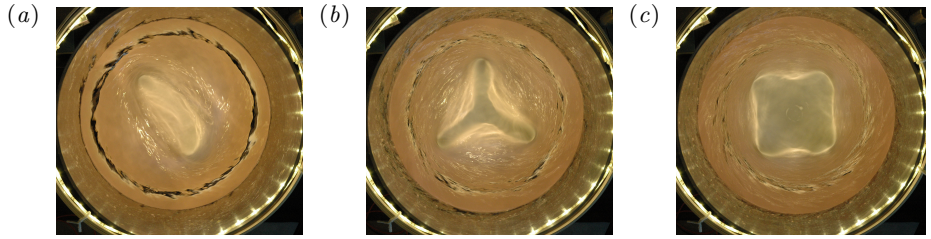

FIGURE 3. Snapshots of the polygons at $H = 60$ mm, $f_c = 0$ Hz and (a) $f_b = 3.4$ Hz, ellipse $(k = 2)$, (b) $f_b = 4.6$ Hz, triangle $(k = 3)$, and (c) $f_b = 5.8$ Hz, square $(k = 4)$.

stationary rotating state. The polygonal states are characterised by noting the number of corners of the stable states. To check for possible multi-stability, a large perturbation of the flow is made by hand to reset the flow, and the number of corners in the resulting state which the flow now finds is also noted. The flow is perturbed between two and five times. The resulting phase diagram is shown in figure 4. The number of corners of the polygonal shape is denoted k. The case $k = 0$ denotes either a circular shape, or that no definite shape could be determined. Each data point consist of two symbols. If these are the same, it means that the state was stable and it kept its polygonal form after the perturbations. If they are different, it means that both states can occur. The left state is the one that appears first and the right one is the most probable alternative state. We have not distinguished between "wet" polygons, where the bottom plate is entirely covered by water (figure 3(a)) and "dry" cases, with a dry central region (figure 3(b)&(c)).

For frequencies higher than 1 Hz polygonal shapes occur (figure 4). Increasing the frequency, they first become elliptical, next triangular, then squares, and finally in some cases pentagonal, before they become unstable, i.e., non-stationary or circular again. The order of polygons for increasing frequencies are consistent with both Vatistas (1990) and Jansson *et al.* (2006). The thresholds for going from one polygon to the next slightly increase with filling height H. Thus the threshold for triangles increases by around 0.5 Hz for each 10 mm water added, and for the threshold of squares it is around 0.8 Hz for each 10 mm water added. The border between different states consists of a transition band with a considerable hysteresis and multi-stability, to which we shall return in section 6. In particular, going from circles to ellipses, there is a large area with unstable states for H between 70 mm and 80 mm, i.e., states that never become fully stationary. Similarly, Vatistas (1990) found that there are transition bands between the different stable polygons, where the shape is a distorted, unstable version of the upper polygonal shape.

Surprisingly, we find a thin bistable band, where squares are also stable, inside the region of triangles for H between 50 mm and 70 mm. For $H = 50$ mm and $H = 60$ mm the triangles were dominating, whereas they were equally likely for $H = 70$ mm. It also looks as if a region of squares is missing after the triangles for $H = 70$ mm but they do not occur in the experiments despite many attempts and long stabilization times. We only find pentagons for $H = 30$ mm, despite many experimental attempts in the areas just above the squares, where we expected to find them. The pentagons found are stable, but it some times took more than five minutes before they stabilised into a regular form. So we can not exclude that they can be found also in other places, but simply did not have enough time to develop.

When the bottom is rotating the water is pushed out from the centre and up against the cylinder wall. The average water height at the cylinder wall, h_c, shown in figure 2, is a measure of the velocity profile. If the flow is close to a line vortex as claimed by Tophøj *et al.* (2013) this height would determine the circulation. In figure 5 we plot the

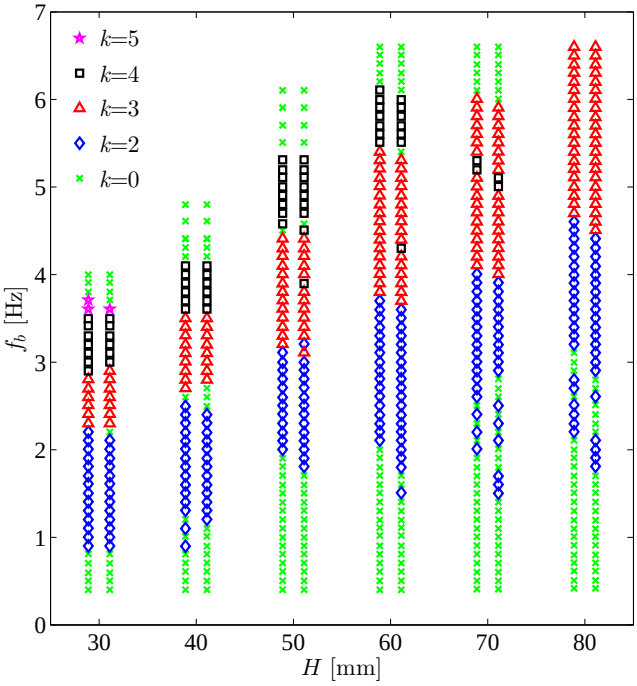

FIGURE 4. Phase diagram in the experiment with rotating bottom plate and stationary cylinder wall. The diagram is spanned by the filling height, H, and the rotational frequency of the bottom plate, f_b. The symmetries of the states are indicated by the symbols in the legend.

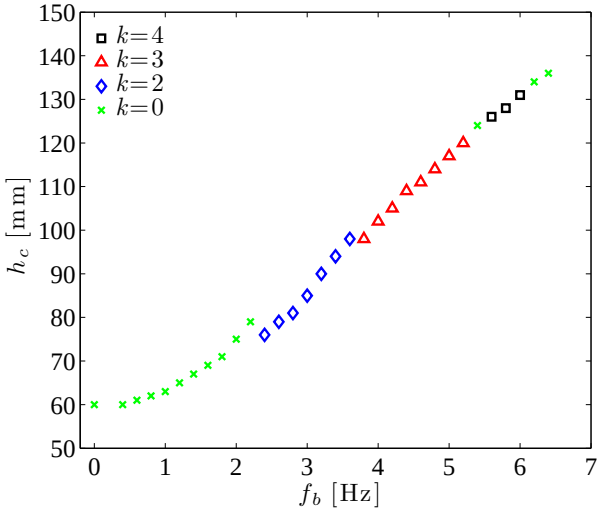

FIGURE 5. The average height of the water at the cylinder wall, h_c as function of the bottom plate frequency, f_b. The cylinder wall was stationary, $f_c = 0$ Hz and the filling height of the water was $H = 60$ mm.

values of h_c against f_b for $H = 60$ mm, i.e., one of the columns in figure 4. The curve is continuous, except at the rotational frequencies where the number of corners change, and even there the change is only a few millimeters. It is interesting that the jumps are always downwards, so one might speculate that the system gains potential energy by adding corners at the appropriate rotational frequency.

4. Combining bottom and cylinder rotation

We now rotate both the bottom plate and the cylinder independently with frequencies f_b and f_c, respectively. In figure 6 we show snapshots of the states going from Newton's bucket, $f_b = f_c$ (figure 6(a)) to the case $f_b = -f_c$ (figure 6(i)), where the bottom and cylinder counter-rotate with the same frequency, by slowly decreasing the cylinder frequency while keeping the bottom frequency constant at $f_b = 2$ Hz. In figure 6(b) we still see no polygon, just a "dry" circular state. The first polygon - a square - forms at $f_c = 0.8$ Hz (figure 6(c)). It is "wet" in the sense that the square contour is covered by water, but it has a dry circular center. The square transforms into a wet triangle at $f_c = 0.4$ Hz (d), and then a wet ellipse at $f_c = 0$ Hz (e). When f_c becomes negative (counter-rotation) the ellipse is destroyed and only a central dent in the surface is left (f) and (g), which becomes smaller and smaller until the water surface seems completely flat (h) and (i). The extreme states, i.e., $f_b = f_c$ and $f_b = -f_c$, are shown from the side in figure 7(a) and figure 7(b), respectively, in this case, for $f_b = 4$ Hz, but with the same filling height ($H = 40$ mm). In the latter case the surface deformation is nearly invisible, despite being disordered by turbulent fluctuations.

In figure 8 we show a phase diagram spanned by f_b and f_c, where we have fixed the filling height at $H = 40$ mm, for which we know from figure 4, that there is a large range of stable states when $f_c = 0$. The bottom frequency f_b was set between 1.0 Hz to 6.5 Hz with steps of 0.5 Hz, and for each of these values f_c was varied with steps of 0.1 Hz. Negative values of f_c indicate that the cylinder is rotating in the opposite sense of the bottom. Note that the horizontal data line for $f_c = 0$ is the same as the vertical data line for $H = 40$ mm in figure 4. The dashed black line is the Newton's bucket flow $f_c = f_b$.

As expected, and confirmed theoretically by Fabre & Mougel (2014), we see no instability at or near the rigidly rotating flow, which appears like a perfect glass bowl (figure 6(a) and figure 7(a)). Actually, the polygon states lie in a wedge-shaped region with predominantly negative values of f_c. For a given bottom frequency the order of appearance of the polygonal states, when the cylinder frequency is increased, is similar to the one we find with the stationary cylinder, and thus we have the same order both vertically and horizontally. From the bottom it is first ellipses; then triangles and then squares, although some shapes are missing for some bottom frequencies. The regions with the same polygonal state are shifted downward in the phase diagram for increasing bottom frequency. For an increase in f_b of 1 Hz the area of, e.g., triangles is shifted down by approximately 0.3 Hz in f_c.

An interesting new feature is the existence of two bands of polygons in figure 8. The lower band only exists at negative f_c and comes into being at $f_b \approx 3.5$ Hz, and thus has no analogue in the $f_c = 0$ phase diagram in figure 4. These polygons are smaller than the ones in the upper band with cylinder frequencies closer to zero, as shown in figure 9. In contrast, polygons in the same band with the same k are known to be different, but predominantly in angles and shapes; not in size (Vatistas 1990). Just like in the case of the polygons with stationary cylinder, the polygons rotate in the same direction as the bottom plate. Surprisingly, the two triangles in figure 9 have essentially the same

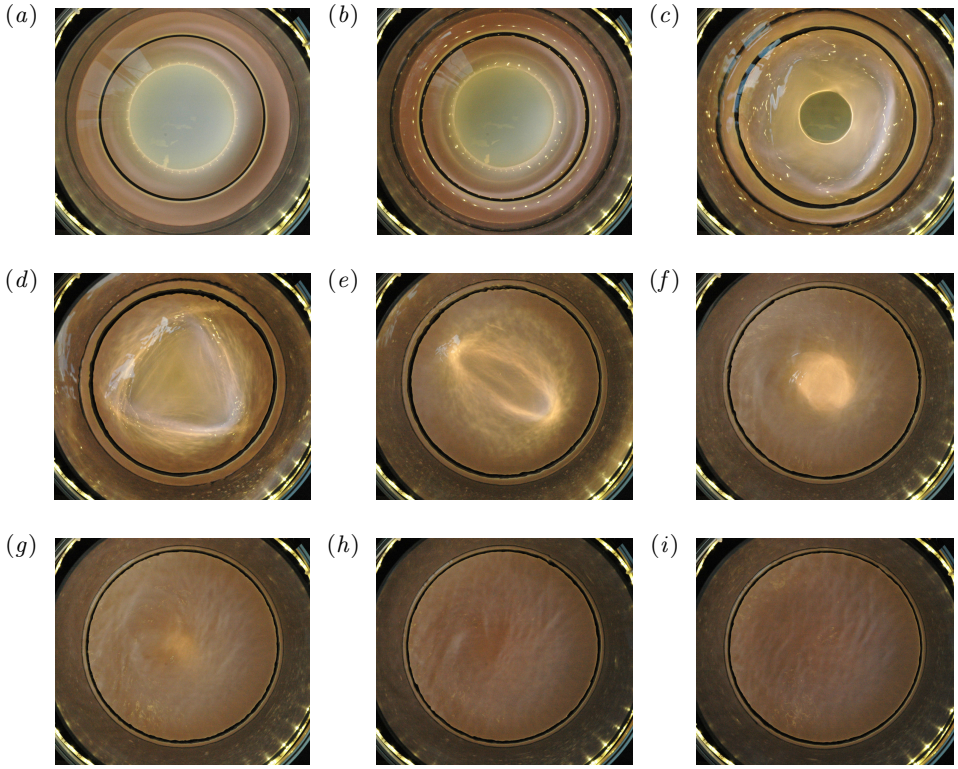

FIGURE 6. Snapshot of the surface states at $H = 40$ mm, $f_b = 2.0$ Hz, and (a) $f_c = 2.0$ Hz, Newton's bucket, (b) $f_c = 1.2$ Hz, circle, (c) $f_c = 0.8$ Hz, square, (d) $f_c = 0.4$ Hz, triangle, (e) $f_c = 0$ Hz, ellipse, (f) $f_c = -0.4$ Hz, central surface dent, (g) $f_c = -0.8$ Hz, central surface dent, (h) $f_c = -1.2$ Hz, flat, and (i) $f_c = -2.0$ Hz, flat.

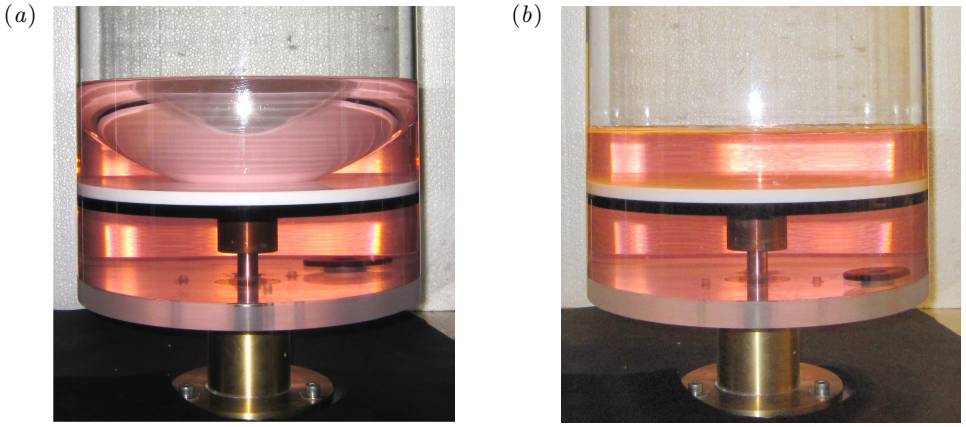

FIGURE 7. (a) Newton's bucket flow, $f_b = f_c = 4$ Hz, where the water is pushed outward from the center due to the centrifugal force. (b) Here $f_b = -f_c = 4$ Hz, and the average water surface is flat, but with strong turbulent fluctuations since the rotation of the cylinder counteracts the influence of the rotation of the bottom plate. In both cases $H = 40$ mm.

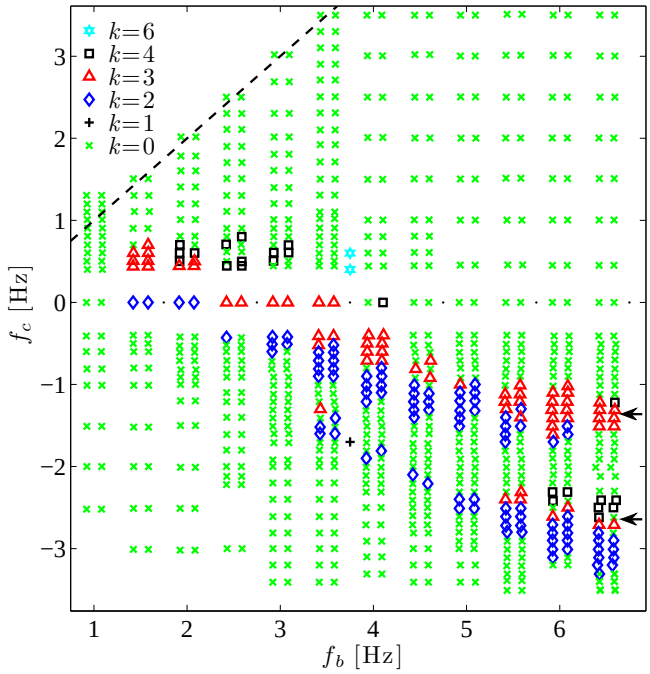

FIGURE 8. Phase diagram of the states at a constant filling height of the water $H = 40$ mm for variable bottom plate frequencies, f_b, and cylinder frequencies, f_c. We have not distinguished between "wet" and "dry" cases. The majority of the polygonal states are found when the cylinder rotates in the opposite direction to the bottom plate. The lower band of states has no counterpart in the system, where only the bottom rotates and has not to our knowledge been described before. The states marked by the arrows are shown in figure 9 which highlight the difference between the two bands. We find hexagons on the line $f_b = 3.75$ Hz and also a monogon ($k = 1$).

rotational frequency, $f_p = (1.15 \pm 0.05)$ Hz, despite their very different sizes and cylinder frequencies that differ by a factor close to two.

An interesting flow is seen in the second band when cylinder and bottom plate counter-rotate at high frequencies. Here, an annular transition region in the flow and surface height is present about 4 cm from the cylinder wall (figure 10). Another unexpected feature of combining bottom plate and cylinder rotation in opposing directions, is the appearance of a dry "monogon", a state with $k = 1$. The monogon is an eccentric circular hole which, contrary to all the other polygons, rotates in the opposite sense of the bottom plate, i.e., with the same sense as the cylinder. It is shown in figure 11 and can be seen "live" in the movie provided in the supplementary material (MonogonMovie 2013).

It also happens, typically near the transition lines, that the system never settles on a stationary state but remains in an unsteady state of which examples are shown in figure 12. In Bergmann *et al.* (2011) it was shown that the formation of a stationary polygonal state can take place via a circular state, and these states are represented as fixed points in figure 13(a). Since the system initially approaches the circular fixed point 'A', it must have many stable directions; although it finally turns out to be a saddle point with a well-defined unstable manifold as sketched in figure 13(a), taking the system off in the direction of the polygon. Similarly the creation of the deformed, non-stationary

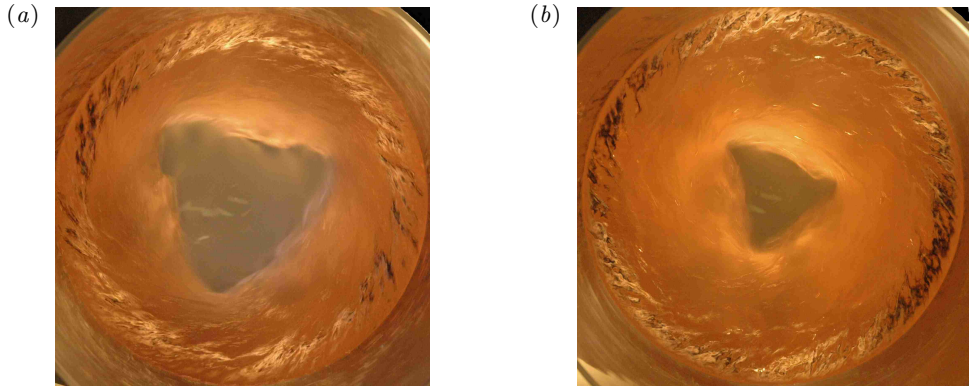

FIGURE 9. Triangles in the two bands at $f_b = 6.5$ Hz and $H = 40$ mm (see arrows in figure 8). (a) at $f_c = -1.4$ Hz (upper band) and (b) $f_c = -2.6$ Hz (lower band). The shapes of the polygons in the two bands are similar, but their size differs by a factor of three. Both polygons rotate in the same direction as the bottom plate, and with similar frequencies, $f_p = (1.15 \pm 0.05)$ Hz.

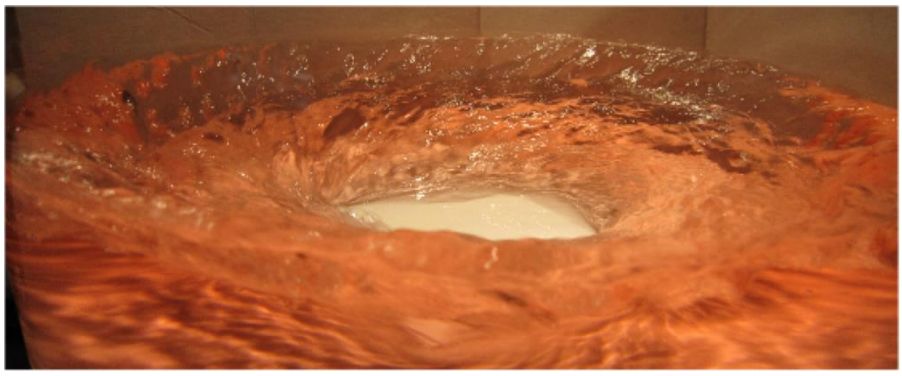

FIGURE 10. Annular transition region when bottom plate and cylinder counter-rotate.

"polygons" seems to take place via first the circular state (figure 12(left)), the saddle point 'A', and then the polygon 'B' in figure 13(a) (e.g., the triangle and pentagon shown in figure 12(center), which now has turned into a weakly unstable saddle point controlling the approach to the final state (figure 12(right)), which, in this case, is not a fixed point, but a non-stationary state represented by something like a strange attractor at 'C' in figure 13(b).

5. Rotation rate and phase of the polygons

We now return to the case in which only the bottom plate rotates. This case has been studied earlier by Vatistas (1990) and Jansson *et al.* (2006) with whom we shall compare our results. In particular, since the dimensions of the set-up in the work by Jansson *et al.* (2006) are the same as in the present experiment, their results should be compatible with ours. We note that in the paper by Jansson *et al.* (2006), which was co-authored by one of us (T.B.), the inner diameter of the cylinder was incorrectly given as 26.2 cm, but in fact it was 29 cm.

In figure 14 the data from figure 4 is plotted with the data from Jansson *et al.* (2006). The two phase diagrams agree qualitatively, but there are quantitative differences

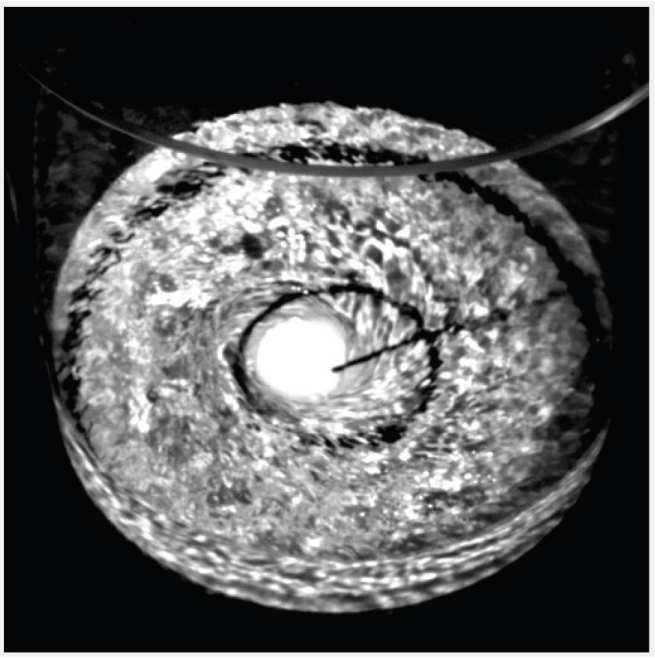

FIGURE 11. The *monogon* is roughly an eccentric circle rotating around the center of the container. It is found near the plus sign in figure 8. The central black circle was painted on the bottom plate. The picture is a snapshot from the movie in the supplementary material.

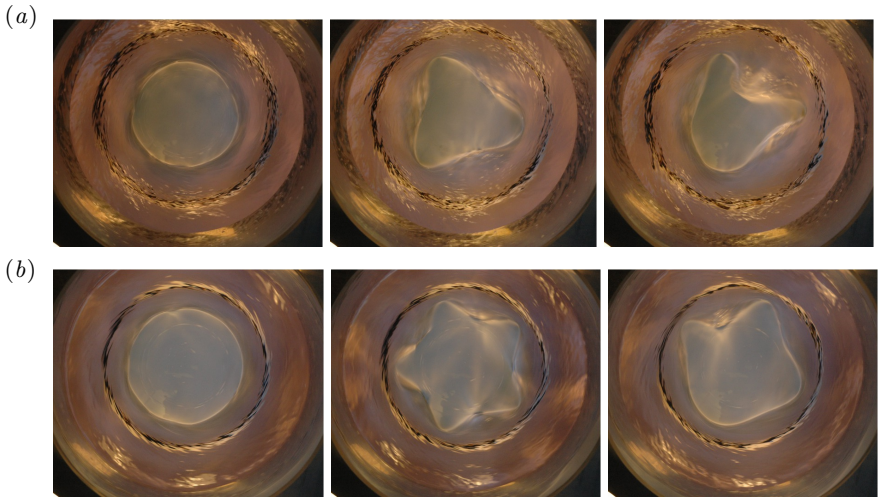

FIGURE 12. Time-series of the formation of an unstable triangle (a) and an unstable pentagon (b). First the flow approaches a circular state (left), then it settles on a regular polygonal state (center), but after a few seconds it becomes irregular (right) and never settles down. The triangle is found at $f_b = 4.0$ Hz, $f_c = 0.44$ Hz and $H = 60$ mm, and the pentagon at $f_b = 4.0$ Hz, $f_c = 1.2$ Hz and $H = 70$ mm.

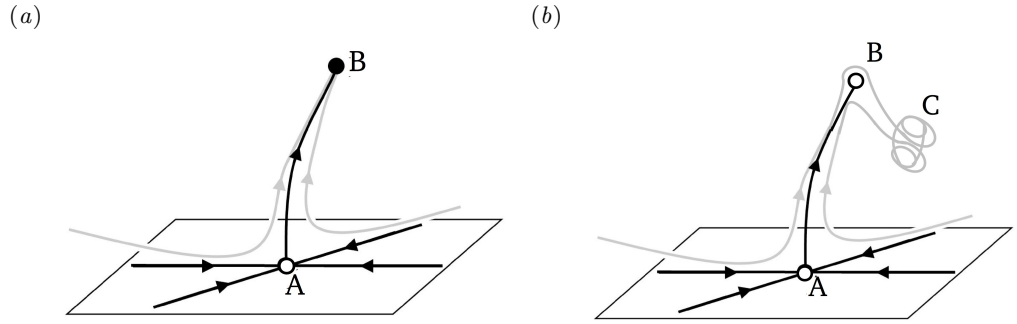

FIGURE 13. (*a*) Phase space for the development of a polygonal state. Initially the system moves towards an almost stable circular shape, A. The fact that A is unstable is felt only very close to it, so from the vicinity of A the system goes off on a well-defined unstable manifold towards a regular stable polygon, B (Bergmann *et al.* 2011). (*b*) Development of the system, when the polygon has become slightly unstable. First it moves toward a circular shape, A, thereafter toward the polygon, B, before it goes off toward something resembling a strange attractor, C, where it remains without settling in a stable state.

between them. All the threshold values are at higher rotational frequencies in our set-up. For example, the band of triangles has been pushed up by approximately 1 Hz. As can also be seen, Jansson *et al.* (2006) found more polygonal states than we do. We only find pentagons for $H = 30$ mm, which, incidentally, is the only filling height where they do *not* find pentagons. Further, they do find hexagons, which we do not unless the cylinder is rotating.

We do not understand the differences between our results and those of Jansson *et al.* (2006). In their experiment, the bottom plate had a vertical wobble motion of approximately 2 mm, whereas ours is less than 0.5 mm. Could the larger misalignment in Jansson *et al.* (2006) actually excite and stabilise the polygon states by a continuing asymmetrical forcing? To answer this we shall provide measurements of the rotational frequencies of the figures and detailed comparison with the rotational frequencies of the plate.

In figure 15 we show the rotation frequencies f_p of some of the polygons as function of the plate frequency f_b at a filling height of $H = 50$ mm. Here we have distinguished between "wet" polygons, where the bottom plate is entirely covered by water (open symbols) and "dry" polygons, where there is a dry central region (filled symbols). If periodic forcing is important, we would expect signs of phase-locking between the bottom plate and the rotating polygon, and we should thus look for rational ratios between f_b and f_p. As seen in figure 15, some of the triangles (in this case the wet ones) have a ratio very close to 1/3, which means that the triangle rotates approximately one corner for every full rotation of the bottom plate and could imply phase-locking between plate and triangle.

To investigate whether the phase of the polygons are actually locked to that of the plate, we have measured their phases accurately. Since it is easier to monitor dry triangles (due to larger contrast), we have decreased the filling height slightly to $H = 40$ mm, where dry triangles with a frequency ratio very close to 1/3 are found. To monitor the phases we make a high-speed recording of the experiment from above. One frame of the resulting movie is shown in figure 16, and it can be seen that the white bottom plate has been painted with a black central circle and a black radial line. To extract quantitative results from the movies, the average value of the pixel intensities in the red box is taken for every frame. If an arm of the triangle is in the red box, this value will be high because a lot of white bottom plate is reflecting the light. That is the case in figure 16. If the arm

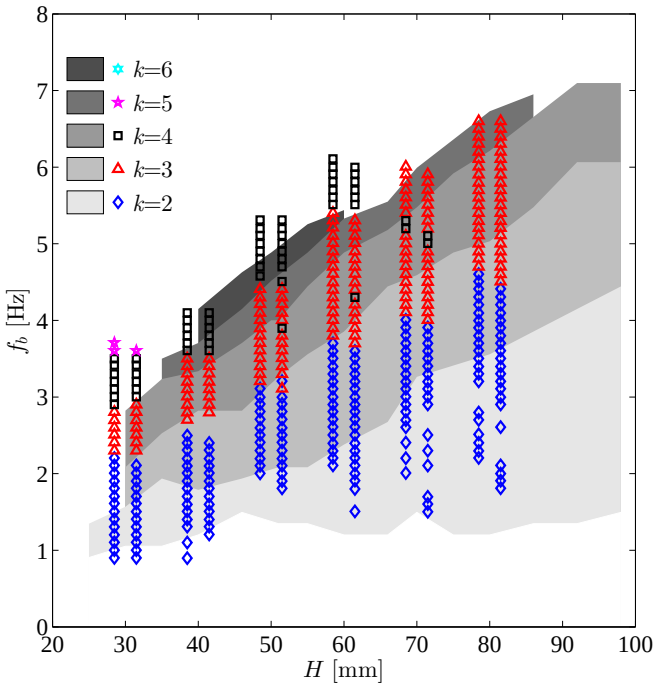

FIGURE 14. Phase diagram with the data in figure 4 (symbols) overlayed on the data by Jansson *et al.* (2006) (greyscale).

is not in the red box, the value will be lower. This gives a measure for the phase and amplitude of the distortion wave. The rotation of the bottom plate can be monitored similarly because for each period, the radial line painted on the bottom plate will pass through the red box once. When it does, the average pixel value will be very low because the line is black.

In figure 17 one can see the results of a measurement of the distortion wave and the bottom plate. As can be seen, the frequency of the figure is close to 1/3 of that of the bottom plate. However, the ratio is not exactly 1/3 and they are not phase locked. The figure shows recordings of the phase of the figure and that of the plate over around 45 rotations of the plate and in this time the phase difference varies by around π. Also, there seems to be no sign of interference between the figure rotation and that of the bottom plate: the amplitude and the distance between two peaks of the polygon remains close to constant throughout the experiment. Figure 18 shows the frequency of the polygon (multiplied by 3) divided by that of the bottom plate versus the frequency of the bottom plate. If there was phase locking, plateaus with constant frequency ratio would appear, but within the accuracy of our experiment they are not seen.

6. Multi-stability and excitability

The surface states show a considerable multi-stability, which is hard to capture in a phase diagram. For most parameters, we find a unique stable state, independently of whether the flow was started from rest or from another state or was perturbed by stirring

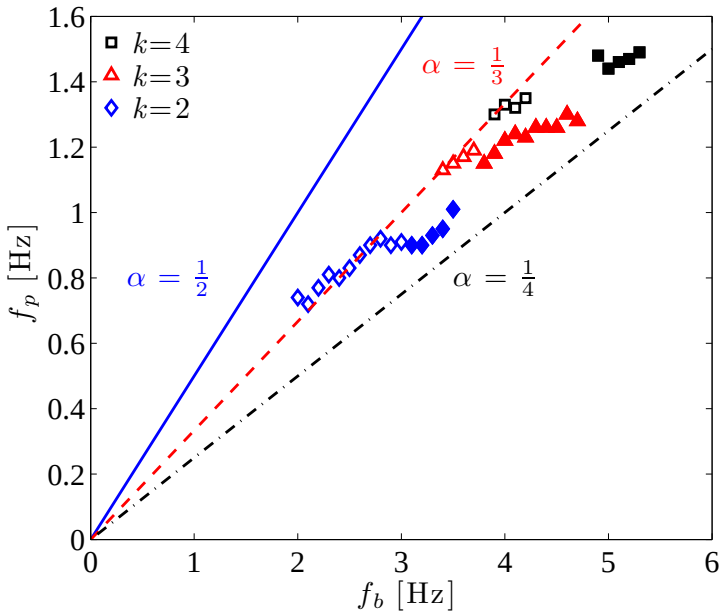

FIGURE 15. The rotational frequency of the polygons, f_p, as function of the rotational frequency of the bottom plate, f_b, with constant water filling height, $H = 50\,\text{mm}$. The dry states have filled markers and the wet states have open markers. The straight lines have the slopes 1/2 (solid), 1/3 (dashed) and 1/4 (dashed-dotted).

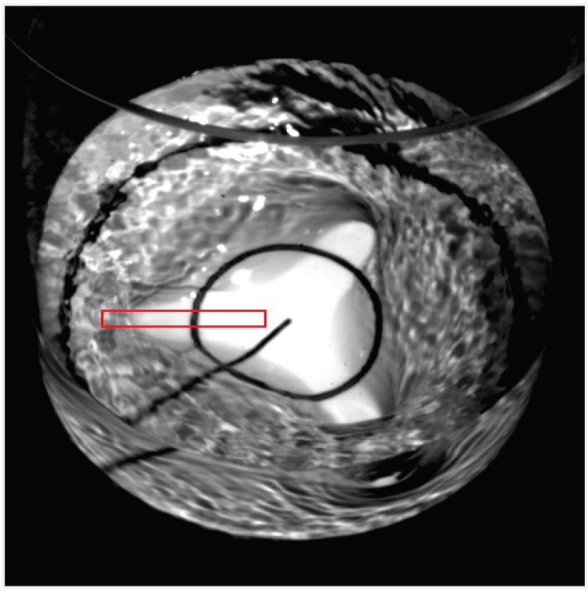

FIGURE 16. Picture from video used to extract the frequency f_b of the bottom plate and the frequency f_p of the polygon, in this case the triangle at $H = 40$ mm and $f_b = 3$ Hz. The plate for this study was painted with a radial line. The average value of the pixels in the red box were used as an indicator of the position of both the figure and the bottom.

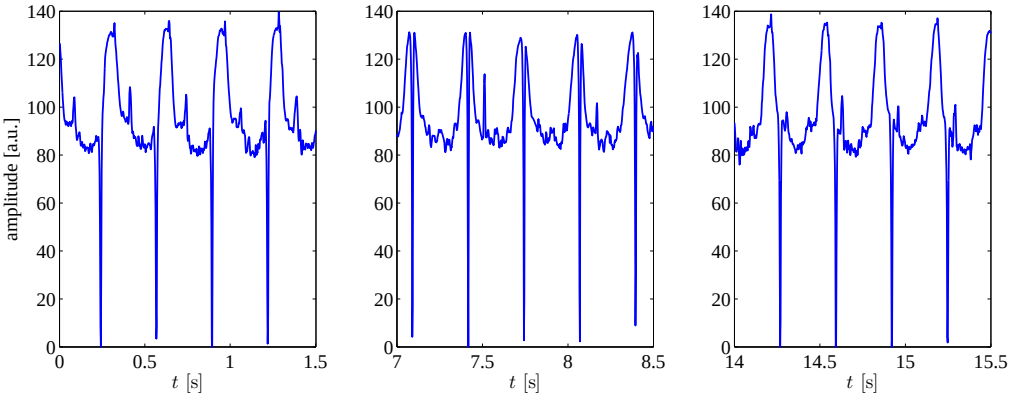

FIGURE 17. The amplitude of the distortion wave describing the triangle and the position of the black radial line on the bottom plate versus time for $H = 40$ mm and $f_b = 3$ Hz. The three figures each show a time interval of the same experiment all in all covering around 45 rotations of the bottom plate. The vertical lines going all the way down signify the bottom plate frequency, whereas the softer upward peaks represent one "arm" or corner of the triangle passing the red box. Taking the three pictures separately, it seems that bottom plate and polygon are phase locked, but combining them it can be seen that they are not, i.e., the phase of the figure is drifting relative to the bottom plate.

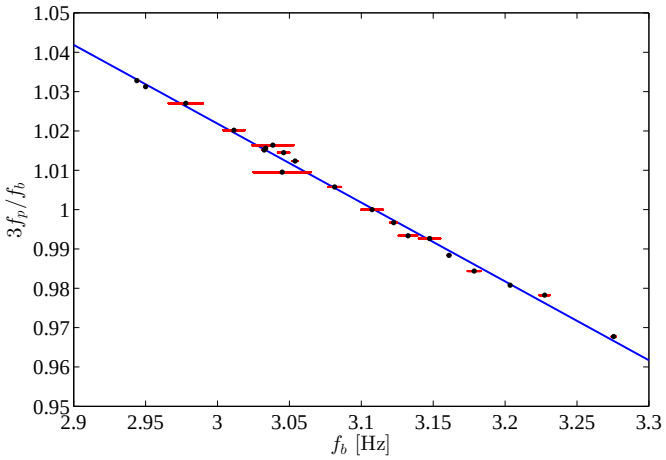

FIGURE 18. Frequency ratio of the polygonal state and the bottom plate, vs. frequency of the bottom plate close to the case $f_p/f_b = 1/3$ with water filling height $H = 40$ mm. It is seen that the frequency-locked case $f_p/f_b = 1/3$ is not preferred over values close by. The dots are the measurement points, the line is a fit and the horizontal lines show the extent of the variation in frequency of the bottom plate during the measurements.

the flow. However, at certain frequencies two or several final states are observed. This happens at the transitional frequencies, where the system changes polygonal state, and there the final state seems rather unpredictable and dependent on small changes in the initial conditions.

In addition to the stable states there are a number of "virtual", almost stable states, which can be excited by slightly perturbing the flow. One way of doing this is to insert a flat, rigid plate vertically into the flow near the rim. According to Tophøj *et al.* (2013),

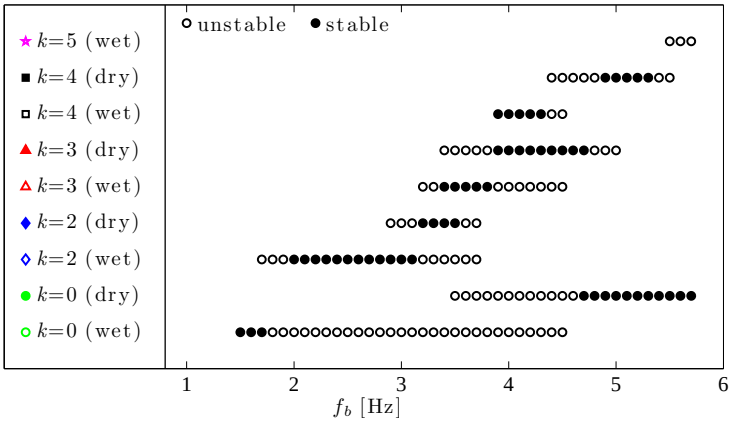

FIGURE 19. Phase diagram with both stable and unstable shapes at filling height $H = 50$ mm. The bottom frequency is along the abscissa and the ordinate shows the appearing shapes at this frequency. Notice that the circular state exists at all bottom frequencies.

the instability forming the polygons stems from resonances between the gravitational waves near the rim of the cylinder and the "centrifugal" waves near the center, and the inserted plate seems to increase the interaction between these waves. As an example, we show in figure 19 the states that we have observed at a filling height of $H = 50$ mm, where the stable states are marked with filled symbols and the unstable ones are open. One can see that at frequencies near $f_b = 3.5$ Hz, it is possible in this way to obtain six different states. We have perturbed the flows both with a ruler held by hand, and with a ruler mounted on a motor, which could flap it along its vertical axis with a given frequency, but the perturbing frequency did not seem to have any strong influence on the possible states. As can be seen, a circular state is always, at least *almost* stable, as also pointed out in Bergmann *et al.* (2011), and it is interesting to note that even this simple state is not unique, since, for some parameters (e.g., around $f_b = 4.25$ Hz), we can have both a wet and a dry circular state coexisting.

It thus appears that the stability and appearance of the polygons can depend strongly on details in the experiment. One such detail, so far not taken into account, appears to be the *temperature*, and we have observed that fewer polygons appear in warm water than in cold water, which probably means that viscosity has an important effect on the stability. Maybe this could explain the difference between the experiments of Jansson *et al.* (2006) and the ones we present, but this should be explored in more detail.

7. Conclusions

We have presented experimental observations of "polygons" on a free fluid surface in a cylindrical container, where the frequency of the bottom plate and the cylinder walls can be varied independently. We have shown that the polygon instability sets in at some distance from the Newton's bucket flow and that the polygons fall in two distinct families: those with low rotation rates of the cylinder, which are related to the ones found earlier and those at large counter-rotation rates which form a new family of smaller sizes. We have compared the case of a stationary cylinder to earlier work, in particular to Jansson *et al.* (2006), and we find a qualitatively similar phase diagram but with considerable quantitative differences. Thus the triangles in our system are found approximately 1 Hz

higher, and we found fewer pentagons and no hexagons as long as the cylinder is stationary. We showed that a triangle rotating at a rate very close to 1/3 of the rotation rate of the plate, has a phase which is not locked to that of the plate, and we conclude that the instability is apparently not driven by small misalignments in our set-up.

For the two-frequency system, we found an additional novel state, a monogon with one "corner" roughly an eccentric circle rotating in the same sense as the cylinder and opposite to that of the plate. The system also displays a considerable multi-stability, in particular near transition points, and we showed that it is possible to excite "virtual" polygons by inserting a plate vertically in the flow. This means that the exact stability properties of the polygons is strongly dependent on details in the experiment and small external perturbations.

We are grateful to Richard Kerswell for suggesting an experiment with independent control of the bottom and cylinder rotations and to Laust Tophøj, Jerome Mougel and David Fabre for discussions of our results. We are also grateful to Knud Aage Mørch and Erik Hansen for helping us with the design of the set-up and to Erik Hansen for his careful work in constructing the set-up. We would like to thank Brdr. Hartmann's Foundation for a grant, which allowed us to build the experiment.

REFERENCES

Aguair, A.C.B, Read, P.L., Wordsworth, R.D., Salter, T. & Yamazaki, Y.H. 2010 A laboratory model of Saturn's north pole hexagon. *ICARUS* **206**, 755–763.

Bergmann, R., Tophøj, L., Homan, T.A.M, Hersen, P., Andersen, A. & Bohr, T. 2011 Polygon formation and surface flow on a rotating fluid surface. *J. Fluid Mech.* **679**, 415–431.

Fabre, D. & Mougel, J. 2014 Generation of three-dimensional patterns through wave interaction in a model of free surface swirling flow. *Fluid Dynamics Research* Submitted.

Godfrey, G.A. 1988 A hexagonal feature around Saturn's north pole. *ICARUS* **76**, 335–356.

Jansson, T.R.N, Haspang, M.R, Jensen, K.H., Hersen, P. & Bohr, T. 2006 Polygons on a rotating fluid surface. *Phys. Rev. Lett.* **96**, 174502.

Lewis, B. M. & Hawkins, H.F. 1982 Polygonal eye walls and rainbands in hurricanes. *Bull. Amer. Meteor. Soc.* **63**, 1294–1301.

MonogonMovie 2013 Movie is available from: `JFM_LINK`.

Suzuki, T., Iima, M. & Hayase, Y. 2006 Surface switching of rotating fluid in a cylinder. *Phys. Fluids* **18**.

Tasaka, Y. & Iima, M. 2009 Flow transitions in the surface switching of rotating fluid. *J. Fluid Mech.* **636** (475), 475–484.

Tophøj, L., Mougel, J., Bohr, T. & Fabre, D. 2013 Rotating polygon instability of a swirling free surface flow. *Phys. Rev. Lett.* **110**, 194502.

Vatistas, G.H. 1990 A note on liquid vortex sloshing and Kelvin's equilibria. *J. Fluid Mech.* **217**, 241–248.

Vatistas, G. H., Abderrahmane, H. A. & Kamran Siddiqui, M. H. 2008 Experimental confirmation of Kelvin's equilibria. *Phys. Rev. Lett.* **100** (174503).